frontiers in Energy Research

ORIGINAL RESEARCH
published: 22 September 2017
doi: 10.3389/fenrg.2017.00025

Analysis of External Surface Irregularities on Fukushima-Derived Fallout Particles

Peter George Martin[1], Yukihiko Satou[2], Ian Griffiths[1], David Richards[3] and Thomas Scott[1]*

[1] Interface Analysis Centre, School of Physics, University of Bristol, HH Wills Physics Laboratory, Bristol, United Kingdom, [2] Collaborative Laboratories for Advanced Decommissioning Science (CLADS), Japan Atomic Energy Agency, Tomioka, Japan, [3] School of Geographical Sciences, University of Bristol, Bristol, United Kingdom

Three large high radioactivity particulate fragments, each several 100 μm in diameter, have been recovered from the region immediately surrounding the Fukushima Daiichi Nuclear Power Plant. Through the application of high-resolution electron and ion-beam methods, this work has sought to investigate the structure and composition of this fibrous surface morphology. By evaluating this, a potential material source can be determined, alongside important information relating to the conditions/events at the time of the reactor explosions and catastrophic release of radioactive materials. The results of this study show that the fibrous features associated with these large radiocesium-containing particles share a common elemental composition. With respect to the surrounding particle, the fibers are enriched in Si, Cl, and Fe, while depleted in both Zn and Al. Based on composition, these fibers are ascribed to thermal insulating material used within the plant, which was sufficiently heated during the loss of coolant incident at the plant to be incorporated into the molten ejecta material that rapidly solidified upon quenching in air. Elemental analysis of these fibers does not reveal any evidence of leaching or the presence of actinide materials.

Keywords: Fukushima Daiichi nuclear disaster, radionuclides, fallout, Fukushima, Nuclear Power Plants, nuclear disaster, contamination

OPEN ACCESS

Edited by:
Muhammad Zubair, University of Sharjah, United Arab Emirates

Reviewed by:
Anca Melintescu, Horia Hulubei National Institute of Physics and Nuclear Engineering, Romania
Barbara Julia Obryk, Institute of Nuclear Physics (PAN), Poland

****Correspondence:***
Peter George Martin
peter.martin@bristol.ac.uk

Specialty section:
This article was submitted to Nuclear Energy, section of the journal Frontiers in Energy Research

Received: *03 August 2017*
Accepted: *05 September 2017*
Published: *22 September 2017*

Citation:
Martin PG, Satou Y, Griffiths I, Richards D and Scott T (2017) Analysis of External Surface Irregularities on Fukushima-Derived Fallout Particles. Front. Energy Res. 5:25. doi: 10.3389/fenrg.2017.00025

INTRODUCTION

Resulting from the Fukushima Daiichi Nuclear Power Plant (FDNPP) accident that occurred during March 2011, a considerable volume of radioactive fallout was deposited onto mainland Japan as well as out into the neighboring Pacific Ocean (Chino et al., 2011; Kawamura et al., 2011). Across the affected Fukushima Prefecture, significant effort is being directed to the remediation of large areas of contaminated fields, forests, and hillslopes—with a total final cost of the clean-up currently estimated at between JPY 1.55 and 16 trillion, depending on the exact level of remediation work to be undertaken (Yasutaka and Naito, 2016). Additional work has, and is continuing, to be directed to the detailed analysis of the form, composition, and environmental behavior of the released material, not only to better understand the events surrounding the incident but also the spread of elemental species within the typhoon-impacted country.

Akin to previous earlier works (Sawhney, 1972; Cremers et al., 1988), most of the radiocesium observed within the environment around the Fukushima Prefecture occurs within fine-scale (sub-micron) soil materials. Studies report preferential Cs sorption onto the interlayers (edge sites) of

both mica and clay-type minerals (Kogure et al., 2012; Mukai et al., 2014; Saito et al., 2014), where it is difficult to disassociate, and is subsequently transported, carried by the host particulate material. Additional studies have also identified Cs within larger material, including 1–2 μm diameter spherical particles (Adachi et al., 2013; Abe et al., 2014; Kogure et al., 2016). Typically employing air-sampling apparatus (located 170 km south west of the facility) in addition to ground-sampled material (tens of kilometers from the plant), some of these studies have also located the existence of uranium species (Martin et al., 2016) within the cores of several of these ejecta fragments (Abe et al., 2014; Kogure et al., 2016).

Whereas some of the material encountered contains actinide species, and others do not, in each instance, the major component of the material analyzed is silicon—constituting the bulk of the material alongside other light and transition elements including C, O, Na, Mg, Al, K, Ca, Fe, and Zn.

In contrast to both the fine-scale colloidal Cs and the micron-sized spherical particles, the material analyzed within this work was collected much closer to the plant (<5 km to the Northwest) and is also orders of magnitude greater in size. Like the smaller spherical particles, however, previous studies have shown that Si is the dominant component alongside the aforementioned accessory elements (Kogure et al., 2016; Satou et al., 2016; Furuki et al., 2017). In contrast—unlike the smaller spherical particles, despite containing radiocesium (detectable *via* standard gamma-spectrometry), the presence of Cs was not identified through energy dispersive spectroscopy (EDS) of the material—but through synchrotron radiation analysis (Ono et al., 2017), illustrating (i) its spatial heterogeneity (despite the inherent low limit of detection) and (ii) its existence within the particle's internal structure.

As part of the analysis carried out on the ejecta materials, scanning electron microscope (SEM) imaging has been performed on both material types (micron-scale spherical and large angular fragments). The external surfaces of the spherical material have been shown to be highly smooth and regular (Adachi et al., 2013; Abe et al., 2014), with the larger-sized particles exhibiting significantly greater angularity and number of surface morphological features (Satou, 2016). Several fragments of particulate on the same micron length-scale of the spherical material, collected at 20 km from the FDNPP, have recently been isolated and found to also exhibit marked angularity (Satou et al., 2016).

Such a contrasting size and form; combined with (i) differing radiocesium ratios ($^{134}Cs/^{137}Cs$) determined in previous works (Chino et al., 2016), (ii) the location at which the samples were obtained and (iii) reactor core modeling (Nishihara et al., 2012), has led many to speculate that each particulate type represents emission from a specific reactor at the Fukushima site (Shibahara et al., 2014; Zheng et al., 2014; Snow et al., 2016).

Work by Salbu and Krekling (1998) analyzing particulate released from the Chernobyl nuclear accident of 1986 observed that the material was not principally silicate but actinide-based—resulting from the explosive break-up of the reactors uranium dioxide core. This high silicate component (and only trace levels of actinides, if any) encountered in the Fukushima-derived samples has been invoked to suggest that limited core release occurred from the events in Japan—with the material arising instead from a hydrogen explosion occurring within the reactor building due to gas build-up inside the reactor pressure vessel (Satou, 2016; Ono et al., 2017).

EXPERIMENTAL

Sample Collection

The bulk material containing the particulate material consisted of dirt collected from the ground at the Cambridge Filter Company (37.4379125N, 141.0222995E) on the 20th August 2016. This site is located on the northwest perimeter boundary of the FDNPP site, 2 km from the coast, and the six reactor buildings of the FDNPP. The material was selected due to the high count rate it exhibited upon examination with a handheld radiation survey meter. Selected material was removed from the grounds surface and placed into a sealed plastic sample bag for transportation and subsequent homogenization (required for sample extraction, below).

Sample Extraction

An initial homogenization of the sample within the plastic sample bag was first performed as per details described fully within Onda et al. (2015). Following this, a step-wise extraction of the particulate exhibiting a high Cs gamma activity occurred, with a full methodology described within Satou et al. (2016). After exposing the sample to an imaging plate, regions not displaying strong radioactive emissions were removed from the sample sheet and the exposure process was repeated on the reduced volume of material. Resulting from the numerous repetitions of this division and exposure process, radioactive particles were finally removed from the surrounding material using a pair of fine-tipped tweezers, before being placed onto an electron microscope (pin) stub for analysis.

The three samples (termed CF-01-1, CF-01-2, and CF-01-3) analyzed during this study were all extracted from the same volume of contaminated sediment material. Each of the particles showed considerable Cs radioactivity—as determined *via* a conventional gamma-ray spectrometer held in proximity to each of the particle-containing analysis stubs.

Electron Imaging and Ion-Beam Milling

Initial imaging of the regions on each of the samples was performed using a Zeiss SIGMA Variable Pressure (VP) Field Emission-SEM (FE-SEM) (Oberkochen, Germany). Through application of the instruments VP function, introducing a nitrogen-rich atmosphere into the instruments, the material was imaged without the requirement for conductive sample coating.

Also installed onto the FE-SEM was an EDAX (Mahwah, NJ, USA) Octane Plus Si-drift EDS detector to undertake compositional analysis of the sample. During sample imaging, a 10 kV, 0.3 nA (30 μm aperture) beam was employed, with the beam parameters increased to 20 kV and 1.2 nA (120 μm aperture) during EDS spectra acquisition. A consistent working distance of 8–10 mm (with 0° sample tilt) was maintained throughout both imaging and EDS analysis. EDS point analysis alongside line scanning and mapping were undertaken during this work.

EDS acquisition was conducted to achieve optimum count rates while maintaining a detector dead-time of approximately 30%. Multiple scan repetitions (line scans and maps) were performed to improve the overall signal to noise ratio.

To determine if a prevailing orientation was present across the identified particles surface fibers, their orientation was determined using the microscopes suite of measurement and image analysis tools, with the sense of rotation defined arbitrarily as the top of the particle. Orientation measurements were grouped into bins, each of 20° increments.

Ion-beam sectioning of regions of interest across each of the sample surfaces were performed using a Helios NanoLab 600i (FEI Company, Hillsboro, OR, USA) dual SEM—focused ion beam (FIB) instrument. As this instrument does not possess a VP function, beam-induced platinum vapor deposition was performed; whereby a gaseous organometallic platinum precursor (Trimethyl-methylcylopentadienyl Platinum-IV) was injected (and subsequently ionized) by rapidly rastering the gallium ion-beam over a large area—forming a thin electrically conductive layer over only the region of interest. Initial ion-beam milling was undertaken across micron-scale regions at 2.7 nA and 30 kV beam current, with progressively decreasing beam energies used to achieve a high quality final surface finish, free of any "curtaining" artifacts typical of ion-beam preparation.

RESULTS AND DISCUSSION

External Particle Form

An image of the entire exterior of one of the particles (CF-01-3) is shown in **Figure 1A**. Apparent is its highly angular form and irregular surface texture. Whereas most of the samples outer surface is smooth, considerable portions are characterized by numerous pits or recesses—each sub-micron to several microns in diameter, typically rounded in form (**Figure 1B**). Also distributed across the particle surfaces are numerous elongate fibrous features (**Figure 1C**). These fibers all vary in their thickness (measured to occur with dimensions from less than 10 μm, through to bulbous portions averaging 30–35 μm in diameter) and total length (varying from short lengths of 50 μm to longer sections over 100 μm). Observable from **Figure 1A** is their mechanism of attachment to the main body of the particle (yellow dashed region), where each of these strands is seen to be physically fused at each of its ends to the particles exterior surface, rather than simply lying across its surface.

Fiber Exterior Composition

The results of EDS point analyses taken across the entirety of all three samples are shown in the three compositional plots of **Figure 2**. Of the elements present within the sample, the

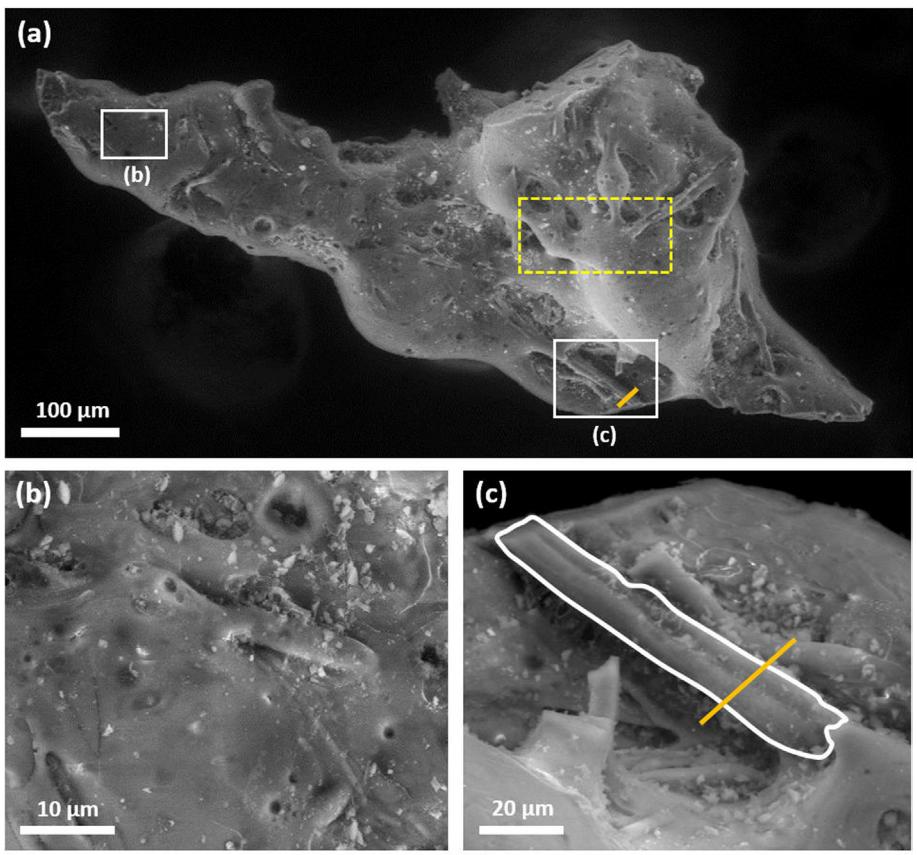

FIGURE 1 | **(A)** Scanning electron microscope image of one of the entire submillimeter particles—apparent is its highly angular form; **(B)** smooth surface region showing micron and sub-micron recesses; **(C)** fibrous surface feature with line of section (**Figures 3A** and **4**) shown.

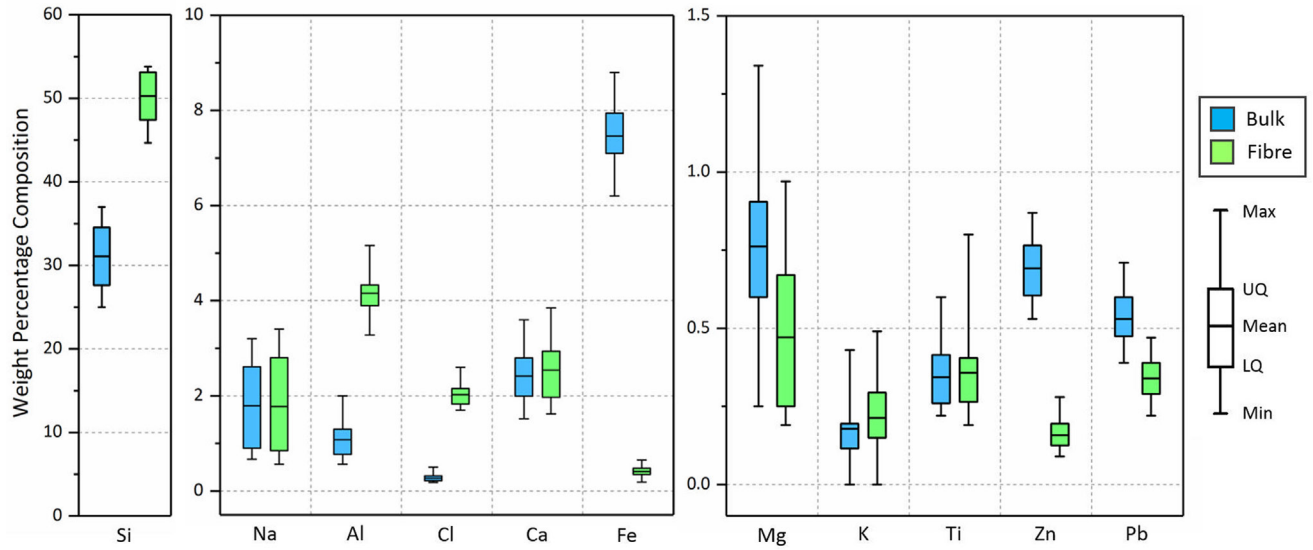

FIGURE 2 | Elemental comparison of both the fibrous regions and surrounding bulk particle. Data from all three particles comprises the results presented in this figure.

most abundant is silicon—with the percentage mass, or weight percentage (wt%), component of this element ranging from 24.9 through to 53.8. Within this range, two distinct clusters can be observed—with Si compositions occurring between 24.9 and 37.1 wt% and 44.6 and 53.8 wt%. This upper range of data points were determined from the fibers that lay across the surface of the particle, whereas the lower values (Si component <37.1 wt%) were all associated with the surrounding bulk of the particle. A similar elemental enrichment for the fibrous component of the material is apparent for Al, where a clear disparity is observed between the bulk particle and the associated surface fiber. As shown in **Figure 2**, the fiber contains more than four times the concentration of aluminum than the material that surrounds it. Also enriched within the particle, however, not at levels as high as for both Si and Al, is the halogen-group element Cl. As is highlighted within **Figure 2**, the fibers all show an elevated Cl content (average: 2.02 wt%) whereas the remainder of the particle contains comparatively little Cl (average: 0.27 wt%).

In contrast, however, some elements show a notable depletion in the fibrous features relative to the particle bulk. The transition elements of iron and zinc (**Figure 2**) both show a large reduction in their concentration across these micron-scale features relative to the material they are contained within. Iron occurs within the fibers with a mean value of 0.41 wt%, whereas away from these structures, the average mass fraction is 7.47 wt%. Similar compositional variation is observed for the zinc, however, to a much lesser extent—with the particle containing an average of 0.16 wt%, and the surrounding bulk 0.69 wt%.

Several elements do not show any discernible difference in their abundance between the background particle and the surface fibers. Both Na and Ca exhibit a wide compositional variation of several weight percent, however, neither element show clearly defined difference between EDS results obtained from the particle or the fibers. The other elements Mg, K, and Ti examined in contrast show a much smaller range in weight percentage composition (<1 wt%), with no significant difference observable between EDS spectra results obtained from both the fiber and surrounding particle regions. A small amount of compositional difference is, however, observed for Pb between the contrasting regions of the sample. However, the degree of overlap is small and could be invoked as an insignificant given the low concentrations of this element (between 0.22 and 0.70 wt%) across both regions. However, Pb is used extensively within nuclear reactors, not just for radiation shielding but also to enclose and surround various core components (due to its ductility), potentially including those insulated with silicon fiber-type materials.

The results of EDS line-scanning across the fibrous structure (position identified in **Figure 1C** of CF-01-03) are shown in **Figure 3A**, detailing the compositional variation for both Si and Zn. As is shown similarly within **Figure 2**, a considerable enrichment in Si is found across the width of the particle above the much-lower levels witnessed within the surrounding particle. A similar depletion of the fiber in Zn, as shown graphically in **Figure 2**, is also shown within the line scan across the fiber. Results from an identical line scan over a thicker fiber (28 μm) are shown within **Figure 3B**. These results are consistent with the smaller fiber (**Figure 3A**), with a considerable enrichment in Si over the surface feature, and a corresponding depletion in Zn over the same scan section.

Combined, these results would suggest a near identical provenance of the material forming the fibers and particle bulk matrix, with the fibers exhibiting a composition slightly higher in silicon and aluminum than the encompassing particle bulk.

Energy dispersive spectroscopy analysis of both the bulk particle and the fibrous features on its surface show no discernible

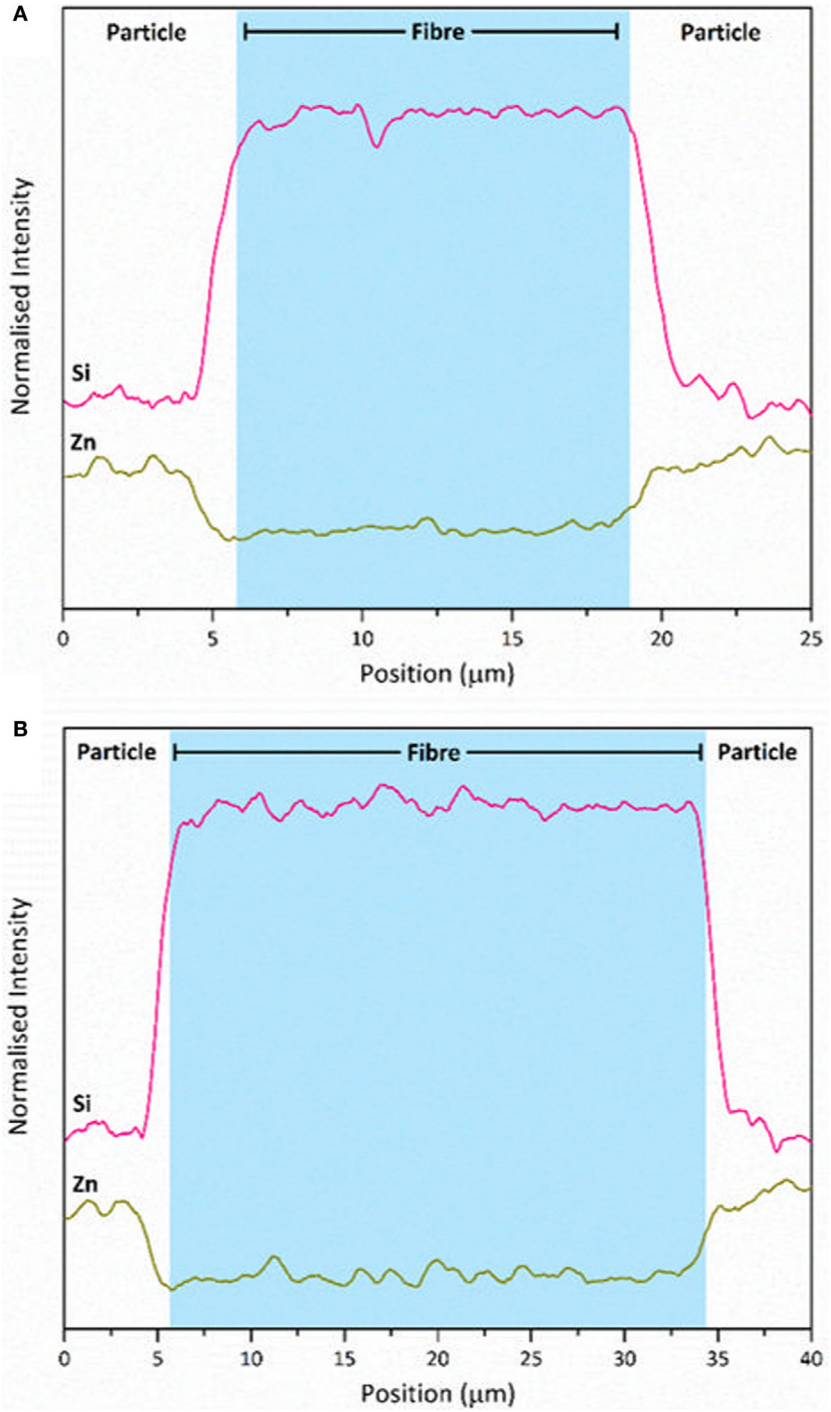

FIGURE 3 | Energy dispersive spectroscopy line scans (Si and Zn) across the fibrous features on particle surfaces; **(A)** line scan over a smaller diameter fiber (as identified in **Figure 1A**); **(B)** line scan over a larger diameter, Si-rich, fiber.

peaks for Cs in any form (radioactive [^{134}Cs and ^{137}Cs] or stable [^{133}Cs]). However, in works conducted on identical samples to these (obtained from the same site), the characteristic gamma-ray emissions of Cs were determined (Satou, 2016) (it is these high-energy gamma-ray photons that were used to initially locate the radioactive material *via* the previously described auto-radiography setup). Resulting from the low sample penetration depth (approximately 2 µm) afforded by EDS analysis (Goldstein et al., 1992)—combined with this gamma-ray spectrometry, it is likely that the radiocesium producing this signal is either; (a) contained at depth below the surface of the particle or more likely (b) at concentrations below that detectable by EDS.

Such a homogenous distribution of radiocesium has been identified in synchrotron analysis of finer-scale (c. 2 μm) Fukushima ejecta material with a greater activity per volume ratio that this larger material. With volatilized Cs present in abundance at the time this material was fused, a consistent spatial distribution is expected.

Fiber Interior Structure and Composition

An SEM image of the results of ion-beam sectioning and sequential low-energy cleaning of the cross-section produced through the region identified in **Figure 1** is shown in **Figure 4A**. From this image, the lack of internal structure within the fibers is apparent—with no microscale crystals or external outer rim or rind at their margins. Toward the top right of the image are two small micron-sized voids, likely representing the location of gaseous inclusions associated with the production of the material.

Elemental EDS mapping of the region imaged in **Figure 4A** is shown in **Figures 4B,C** for Si and Al, respectively. From these maps, the uniform distribution of silicon along the external surface as well as through the fibers interior is apparent. The reduced levels of Si present within the bulk region immediately surrounding the particle is also evident, supporting the line scan EDS results presented in **Figures 3A,B**. Whereas Al is witnessed to have a similar enrichment within the fibers in comparison to the containing particle, as shown formerly in the plot of **Figure 2**, a contrast is apparent within **Figure 4C** between the outermost surface and the fibers interior. Further EDS line scans were undertaken to quantify this compositional consistency, as is the case of Si and heterogeneity—as observed for Al. The resulting line-scan for Si is shown within **Figure 4D** and supports these earlier findings—with the weight percentage of Si consistent (averaging 58 wt%), from the fibers center through to its exterior surface. In contrast, whereas the line scan of Al shows that the concentration within the fibers sectioned core is constant (**Figure 4E**)—a marked increase in Al concentration is observed (as per the EDS map and line scan) with respect to its external surface. Not existing at levels as high as Si, the ion-beam sectioned surface of the fiber contains approximately 5 wt% Al, with the outer-layer containing marginally more—at approximately 7 wt% Al.

Fiber Form and Origin

Acting also as an indicator to the materials provenance—although not as powerful as composition, the orientation of these features across the materials surface could yield information regarding the conditions of formation. A rose diagram detailing the orientations of the fibers encountered across the surface of the fragment sample is shown in **Figure 5**. From this plot, the spread of fiber orientations appears uniform.

This orientation distribution may, therefore, suggest that the fibrous features that occur across the surfaces of these particles are the result of a source fibrous material that itself has a heterogeneous distribution of individual fiber orientations. Or conversely, the fibers may be the result of an explosive or violent emission event, responsible for producing such an orientation variance.

Combining these structural (fiber orientation) results with those compositional results obtained in earlier sections, the

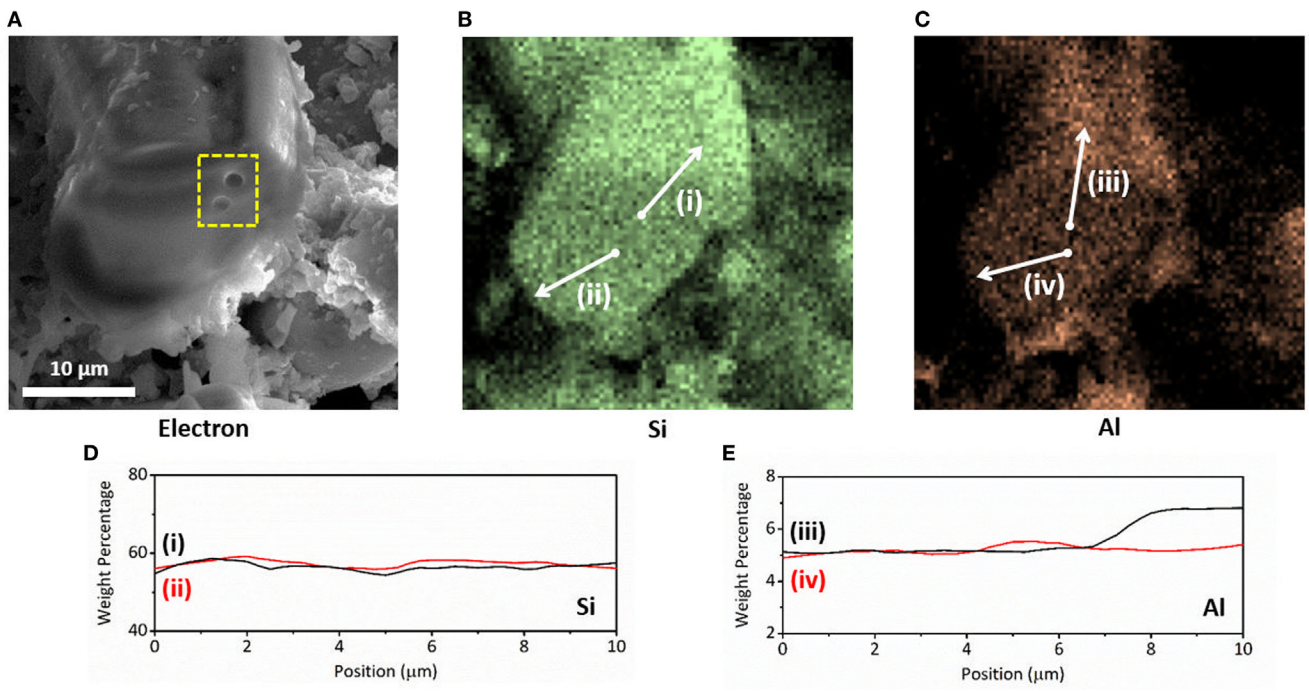

FIGURE 4 | Internal compositional analysis of a surface fiber: **(A)** scanning electron microscope image through a sectioned fiber, the highly amorphous/structureless internal form of the material is apparent alongside two small voids (highlighted); **(B)** energy dispersive spectroscopy (EDS) elemental map of Si distribution; **(C)** EDS elemental map of Al distribution; **(D)** Si compositional line-scans (i) and (ii) as shown in **(B)**; **(E)** Al compositional line-scans (iii) and (iv) as shown in **(C)**.

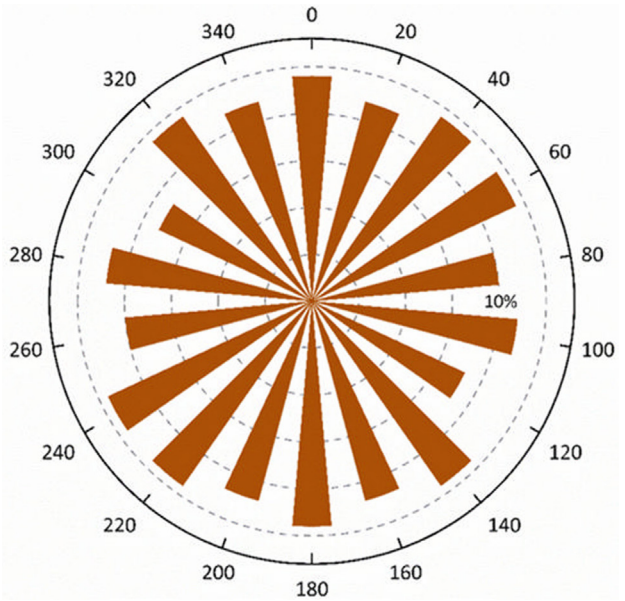

FIGURE 5 | Rose diagram detailing the orientations of the silicon-dominant fibers found on the surface of the particles (arbitrary zero direction).

TABLE 1 | Details of the mean fiber length of silicate insulation materials obtained from prior studies on their physical form (and in some instances, elemental composition).

Study	Mean fiber diameter (μm)
Öztürk (2010)	8–20
Zihlif and Ragosta (2003)	2–25
Rockwool Limited (2017)	4–5
IARC Working Group on the Evaluation of Carcinogenic Risk to Humans (1988)	6–15[a]
IARC Working Group on the Evaluation of Carcinogenic Risk to Humans (1988)	<3.0[b]
Klingholz (1977)	4–6
This work	6–32 (average: 12)

[a]*General thermal insulation.*
[b]*High-temperature thermal insulation.*

likely origin of these surface fibers (as well as the underlying bulk particle sample) can be determined/estimated with respect to the plant as well as the March 2011 events at the FDNPP. The highly fibrous nature of the silicon-rich material, originating from a nuclear plant setting, would strongly invoke the source of the fibers to be insulation-type material. Thermal lagging materials are encountered within reactor buildings such as at the FDNPP, where they insulate the extensive piping network used to transfer steam and pressurized water around the plant. This insulation material occurred more extensively at the FDNPP above the reactor service floor alongside the concrete superstructure of the facility.

For a simplistic comparison of likely source-material, the form of several different commonly encountered insulation materials is presented in **Table 1**. From this table, a strong degree of similarity can be observed between the fibers encountered on the particles external surfaces and those of commonly used insulation materials. The average fiber diameter measured was 12 μm (range: 6–32), with typical values of reported insulation-type materials varying from 2 up to 25 μm. In contrast to the general silicon insulation material reported in the study by the IARC Working Group on the Evaluation of Carcinogenic Risk to Humans (1988) and that of the basalt-based fire-proof silicon composition insulation Rockwool™ (Rockwool Limited, 2017), the maximum thicknesses of these fibers are slightly larger (maximum of 5 and 15 μm, respectively). Such an observed diameter increase/fiber widening (**Figure 1**) may be the result of partial melting of the principally silicate fibers, allowing for the material to flow under the extreme temperatures likely experienced during the in-reactor explosion. The existence of the extensive micron-sized pits across the surface of the particle and fiber (**Figure 1B**) may represent the location of vesicles, or pockets of gas incorporated, and subsequently released from the material during its initial production or during the accident—whereby reactor and fission product gases were incorporated into the sample.

CONCLUSION

Analysis of the particulate material presented in this study has allowed for a far greater understanding of the likely source of these submillimeter radioactive particles found in the environment surrounding the FDNPP. The analysis also provides greater insight into the events that occurred during March 2011 as the reactor facility experienced multiple different loss of coolant incidents with ensuing reactor building explosions.

The large size of the particulate material collected near the reactor site, coupled with its highly angular nature is strongly indicative of a highly energetic mechanism of formation—explosive in nature; consistent with the events described during the numerous accounts of the incident by the media. Principally, a large-scale hydrogen explosion resulting from the ignition of hydrogen gas following the highly exothermic oxidation of the zircalloy fuel cladding material at the elevated reactor temperatures.

After compositional and structural analysis of the bulk particle material, the main constituent element was observed to be silicon. In contrast, the fibers, which truncated the surface themselves were characterized by elevated levels of Si, Al, and Cl alongside depleted levels of Zn and Fe (and potentially Pb). With a radiocesium signal determined *via* gamma-ray spectrometry, EDS analysis of the sample surfaces, however, did not yield such compositional results for Cs. As such, this Cs is (a) ascribed to be located at greater depth within the particles interior, where upon emission as a super-heated volatile species from the hydrogen explosions, it was rapidly quenched and encased within the "rind" of silicon evidenced in this work or (b), at concentrations well below those of EDS analysis. Compositional analysis has shown that certain species are concentrated/depleted in specific regions with respect to others. This most-likely represents the state at the initial formation of the material but may potentially also result due to the influence of species leaching by environmental waters.

Further work to investigate the internal form and chemistry of the material will utilize synchrotron radiation techniques. Such

studies will aim to evaluate the environmental fate of material through assessing whether there is potential for various species to leach out under environmental conditions typical of the region.

The remediation of the region from which this material was obtained (located close to the boundary with the plant) is not set to begin for a considerable period of time (METI, 2015). While primarily composed of Si, with the radioactivity attributed to Cs (which itself is rapidly decaying to various stable isotopes), being sourced from close to the reactors core, the proposed synchrotron studies of the particles internal form and composition will be hugely important. Through this assessment as to whether actinide species are present at the particle center will ultimately dictate the clean-up strategy in the region close to the plant.

AUTHOR CONTRIBUTIONS

All authors contributed to the final manuscript. PM, YS, and IG performed the analysis of the sample material. DR and TS supervised the study.

ACKNOWLEDGMENTS

The authors thank Dr. Keisuke Sueki and Mr. Kazuki Matsuo—University of Tsukuba (sample collection and initial analysis). The authors also thank Dr. Haruka Minowa—Jikei University (sample collection), Dr. Hideki Yoshikawa, and Dr. Shigeo Nakama at Fukushima—Environmental Safety Centre, JAEA (sample collection).

FUNDING

The authors wish to thank the kind funding provided by the Daiwa Anglo-Japanese Foundation (Reference: 11424) as well as the Great Britain Sasakawa Foundation (Reference: 5223) that allowed for this work. Additional support of the JAEA to allow for the visit of YS to the University of Bristol is gratefully acknowledged. The electron microscope used in this work was provided on an instrument purchased with support from the EPSRC (Reference: EP/K040340/1).

REFERENCES

Abe, Y., Iizawa, Y., Terada, Y., Adachi, K., Igarashi, Y., and Nakai, I. (2014). Detection of uranium and chemical state analysis of individual radioactive microparticles emitted from the Fukushima nuclear accident using multiple synchrotron radiation X-ray analyses. *Anal. Chem.* 86, 8521–8525. doi:10.1021/ac501998d

Adachi, K., Kajino, M., Zaizen, Y., and Igarashi, Y. (2013). Emission of spherical cesium-bearing particles from an early stage of the Fukushima nuclear accident. *Sci. Rep.* 3, 2554. doi:10.1038/srep02554

Chino, M., Nakayama, H., Nagai, H., Terada, H., Katata, G., and Yamazawa, H. (2011). Preliminary estimation of release amounts of 131I and 137Cs accidentally discharged from the Fukushima Daiichi Nuclear Power Plant into the atmosphere. *J. Nucl. Sci. Technol.* 48, 1129–1134. doi:10.1080/18811248.2011.9711799

Chino, M., Terada, H., Nagai, H., Katata, G., Mikami, S., Torii, T., et al. (2016). Utilization of 134Cs/137Cs in the environment to identify the reactor units that caused atmospheric releases during the Fukushima Daiichi accident. *Sci. Rep.* 6, 31376. doi:10.1038/srep31376

Cremers, A., Elsen, A., De Preter, P., and Maes, A. (1988). Quantitative analysis of radiocaesium retention in soils. *Nature* 335, 247–249. doi:10.1038/335247a0

Furuki, G., Imoto, J., Ochiai, A., Yamasaki, S., Nanba, K., Ohnuki, T., et al. (2017). Caesium-rich micro-particles: a window into the meltdown events at the Fukushima Daiichi Nuclear Power Plant. *Sci. Rep.* 7, 42731. doi:10.1038/srep42731

Goldstein, J. I., Newbury, D. E., Echlin, P., Joy, D. C., Romig, A. D., Lyman, C. E., et al. (1992). *Scanning Electron Microscopy and X-Ray Microanalysis: A Text for Biologists, Materials Scientists, and Geologists*, 2nd Edn. New York: Plenum Press.

IARC Working Group on the Evaluation of Carcinogenic Risk to Humans. (1988). *IARC Monographs Programme on the Evaluation of Carcinogenic Risks to Humans: Man-Made Mineral Fibres*. Lyon: International Agency for Research on Cancer.

Kawamura, H., Kobayashi, T., Furano, A., In, T., Ishikawa, Y., Nakayama, T., et al. (2011). Preliminary numerical experiments on oceanic dispersion of 131 I and 137 Cs discharged into the ocean because of the Fukushima Daiichi Nuclear Power Plant disaster. *J. Nucl. Sci. Technol.* 48, 1349–1356. doi:10.1080/18811248.2011.9711826

Klingholz, R. (1977). Technology and production of man-made mineral fibres. *Ann. Occup. Hyg.* 20, 153–159. doi:10.1093/annhyg/20.2.153

Kogure, T., Morimoto, K., Tamura, K., Sato, H., and Yamagishi, A. (2012). XRD and HRTEM evidence for fixation of cesium ions in vermiculite clay. *Chem. Lett.* 41, 380–382. doi:10.1246/cl.2012.380

Kogure, T., Yamaguchi, N., Segawa, H., Mukai, H., Motai, S., Akiyama-Hasegawa, K., et al. (2016). Constituent elements and their distribution in the radioactive Cs-bearing silicate glass microparticles released from Fukushima nuclear plant. *Microscopy* 65, 451–459. doi:10.1093/jmicro/dfw030

Martin, P. G., Griffiths, I., Jones, C. P., Stitt, C. A., Davies-Milner, M., Mosselmans, J. F. W., et al. (2016). In-situ removal and characterisation of uranium-containing particles from sediments surrounding the Fukushima Daiichi Nuclear Power Plant. *Spectrochim. Acta Part B At. Spectrosc.* 117, 1–7. doi:10.1016/j.sab.2015.12.010

METI. (2015). *Areas to Which Evacuation Orders Have Been Issued [WWW Document]*. Available at: http://www.meti.go.jp/english/earthquake/nuclear/roadmap/pdf/150905MapOfAreas.pdf

Mukai, H., Hatta, T., Kitazawa, H., Yamada, H., Yaita, T., and Kogure, T. (2014). Speciation of radioactive soil particles in the Fukushima contaminated area by IP autoradiography and microanalyses. *Environ. Sci. Technol.* 48, 13053–13059. doi:10.1021/es502849e

Nishihara, K., Iwamoto, H., and Suyama, K. (2012). *Estimation of Fuel Compositions in Fukushima-Daiichi Nuclear Power Plant*. Tokyo: JAEA.

Onda, Y., Kato, H., Hoshi, M., Takahashi, Y., and Nguyen, M.-L. (2015). Soil sampling and analytical strategies for mapping fallout in nuclear emergencies based on the Fukushima Dai-ichi Nuclear Power Plant accident. *J. Environ. Radioact.* 139, 300–307. doi:10.1016/j.jenvrad.2014.06.002

Ono, T., Yushin, I., Abe, Y., Nakai, I., Terada, Y., Satou, Y., et al. (2017). Investigation of the chemical characteristics of individual radioactive microparticles emitted from reactor 1 by the Fukushima Daiichi Nuclear Power Plant accident by using multiple synchrotron radiation X-ray analyses. *Bunseki Kagaku* 66, 251–261. doi:10.2116/bunsekikagaku.66.251

Öztürk, B. (2010). Hybrid effect in the mechanical properties of jute/rockwool hybrid fibres reinforced phenol formaldehyde composites. *Fibers Polym.* 11, 464–473. doi:10.1007/s12221-010-0464-3

Rockwool Limited. (2017). *Deleterious Materials Data Sheet* Cardiff. Available at: http://www.rockwool.co.uk/technical-support/documentation/datasheets/

Saito, T., Makino, H., and Tanaka, S. (2014). Geochemical and grain-size distribution of radioactive and stable cesium in Fukushima soils: implications for their long-term behavior. *J. Environ. Radioact.* 138, 11–18. doi:10.1016/j.jenvrad.2014.07.025

Salbu, B., and Krekling, T. (1998). Characterisation of radioactive particles in the environment. *Analyst* 123, 843–850. doi:10.1039/a800314i

Satou, Y. (2016). *Study of Relationship between Deposition of Radioactive Materials and Radioactive Particles in the Difficult-to-Return Zone Caused by the Fukushima Dai-ichi Nuclear Power Plant Accident*. Tsukua: University of Tsukuba.

Satou, Y., Sueki, K., Sasa, K., Adachi, K., and Igarashi, Y. (2016). First successful isolation of radioactive particles from soil near the Fukushima Daiichi Nuclear Power Plant. *Anthropocene* 14, 71–76. doi:10.1016/j.ancene.2016.05.001

Sawhney, B. L. (1972). Selective sorption and fixation of cations by clay minerals. A review. *Clays Clay Miner.* 20, 93–100. doi:10.1346/CCMN.1972.0200208

Shibahara, Y., Kubota, T., Fujii, T., Fukutani, S., Ohta, T., Takamiya, K., et al. (2014). Analysis of cesium isotope compositions in environmental samples by thermal

ionization mass spectrometry – 1. A preliminary study for source analysis of radioactive contamination in Fukushima Prefecture. *J. Nucl. Sci. Technol.* 51, 575–579. doi:10.1080/00223131.2014.891954

Snow, M. S., Snyder, D. C., and Delmore, J. E. (2016). Fukushima Daiichi reactor source term attribution using cesium isotope ratios from contaminated environmental samples. *Rapid Commun. Mass Spectrom.* 30, 523–532. doi:10.1002/rcm.7468

Yasutaka, T., and Naito, W. (2016). Assessing cost and effectiveness of radiation decontamination in Fukushima Prefecture, Japan. *J. Environ. Radioact.* 151, 512–520. doi:10.1016/j.jenvrad.2015.05.012

Zheng, J., Tagami, K., Bu, W., Uchida, S., Watanabe, Y., Kubota, Y., et al. (2014). 135Cs/137Cs isotopic ratio as a new tracer of radiocesium released from the Fukushima nuclear accident. *Environ. Sci. Technol.* 48, 5433–5438. doi:10.1021/es500403h

Zihlif, A. M., and Ragosta, G. (2003). A study on the physical properties of rock wool fiber—polystyrene composite. *J. Thermoplast. Compos. Mater.* 16, 273–283. doi:10.1177/0892705703016003005

Conflict of Interest Statement: The authors declare that the research was conducted in the absence of any commercial or financial relationships that could be construed as a potential conflict of interest.